Advances in Theoretical Studies of Electron Capture

Sevestrean Vasile-Alin

26 May 2026

Table of Contents

Electron Capture (EC)

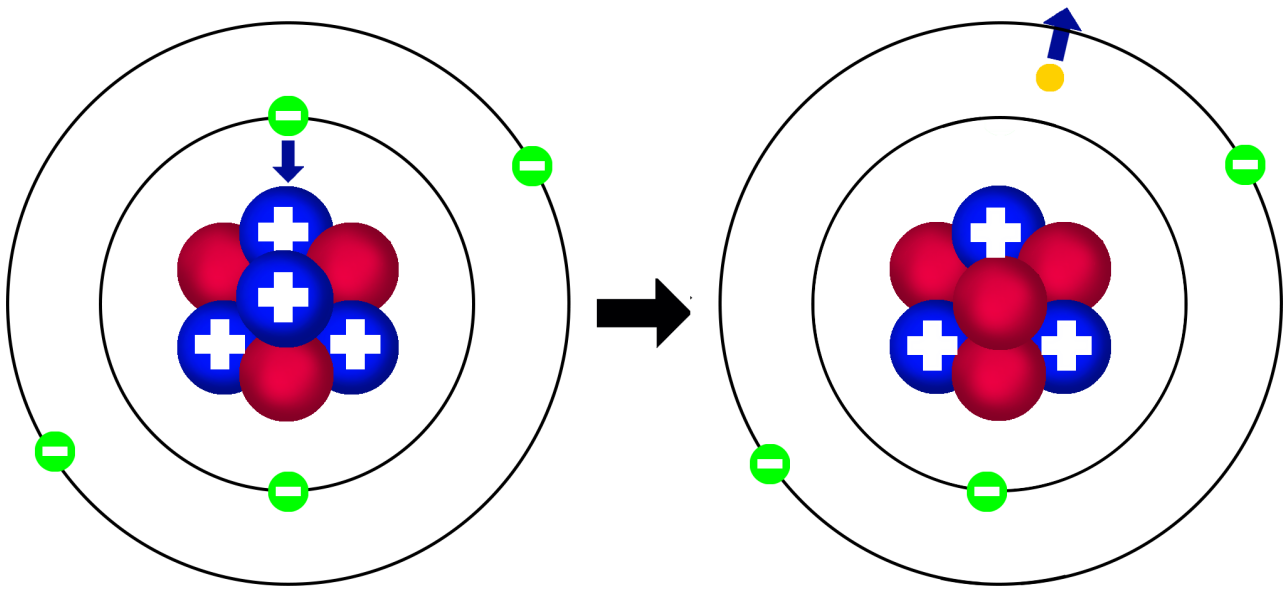

Figure: Electron Capture

Why EC?

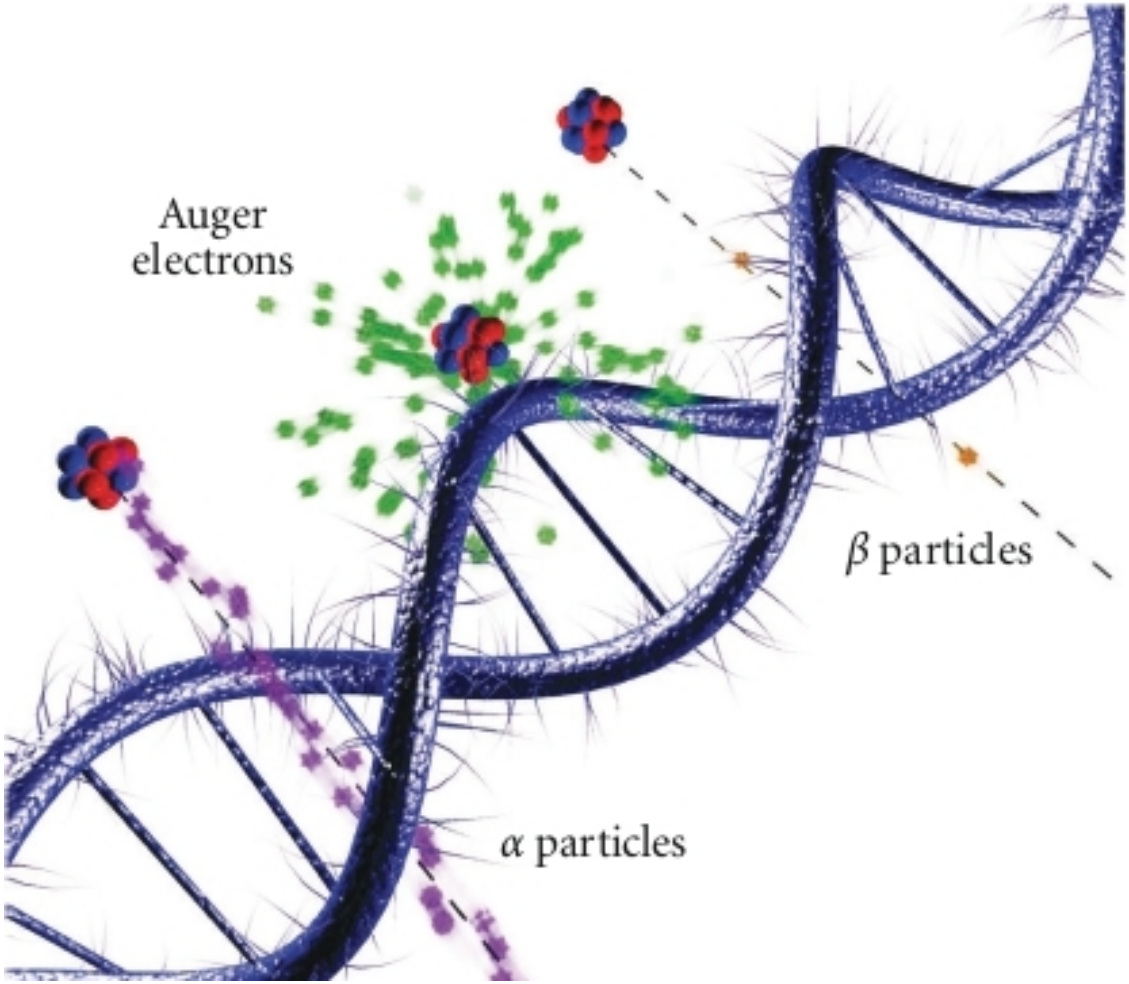

Figure: EC in Nuclear medicine [1]

Why EC?

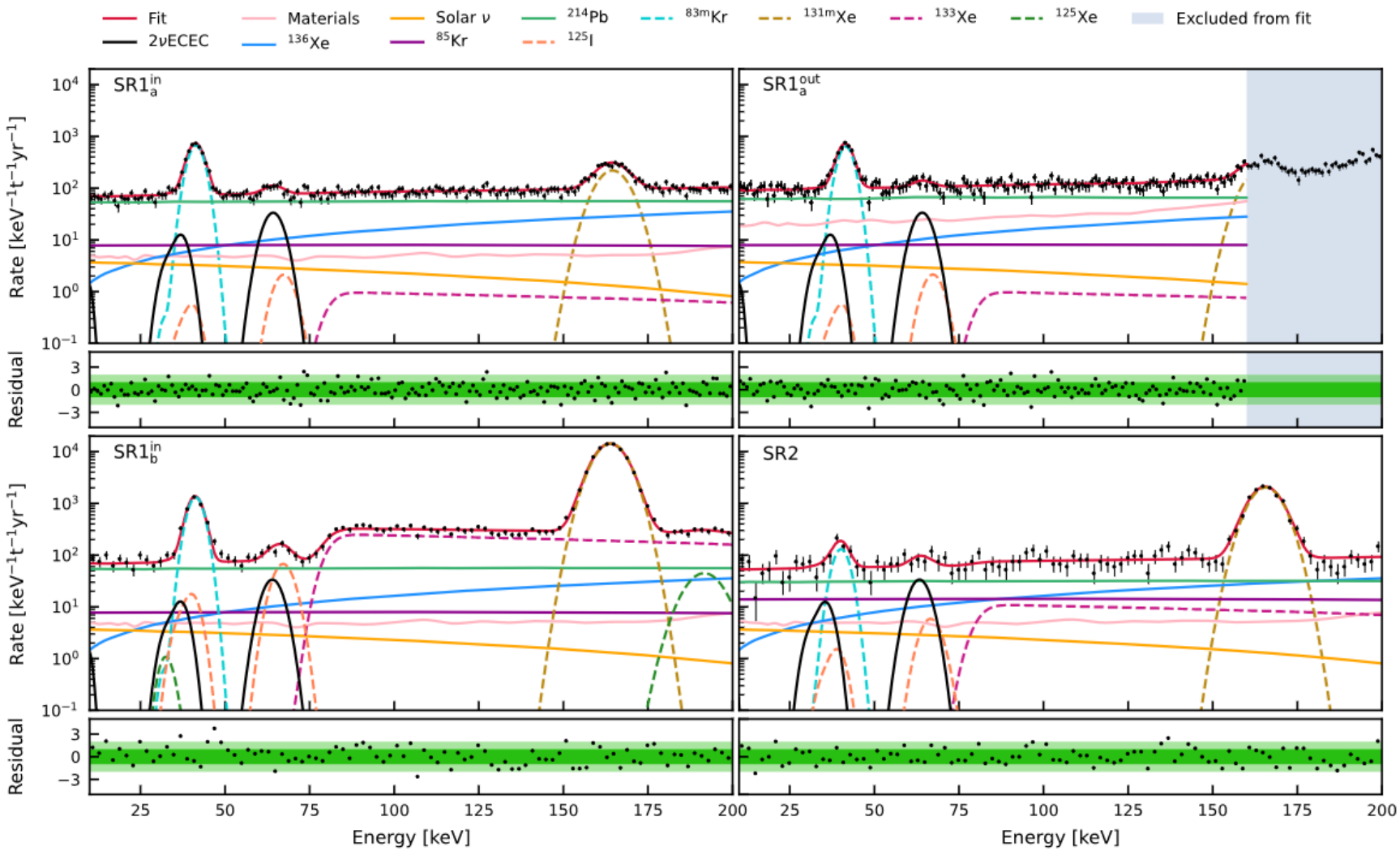

Figure: XENON1T Collaboration experimental results [2]

Why EC?

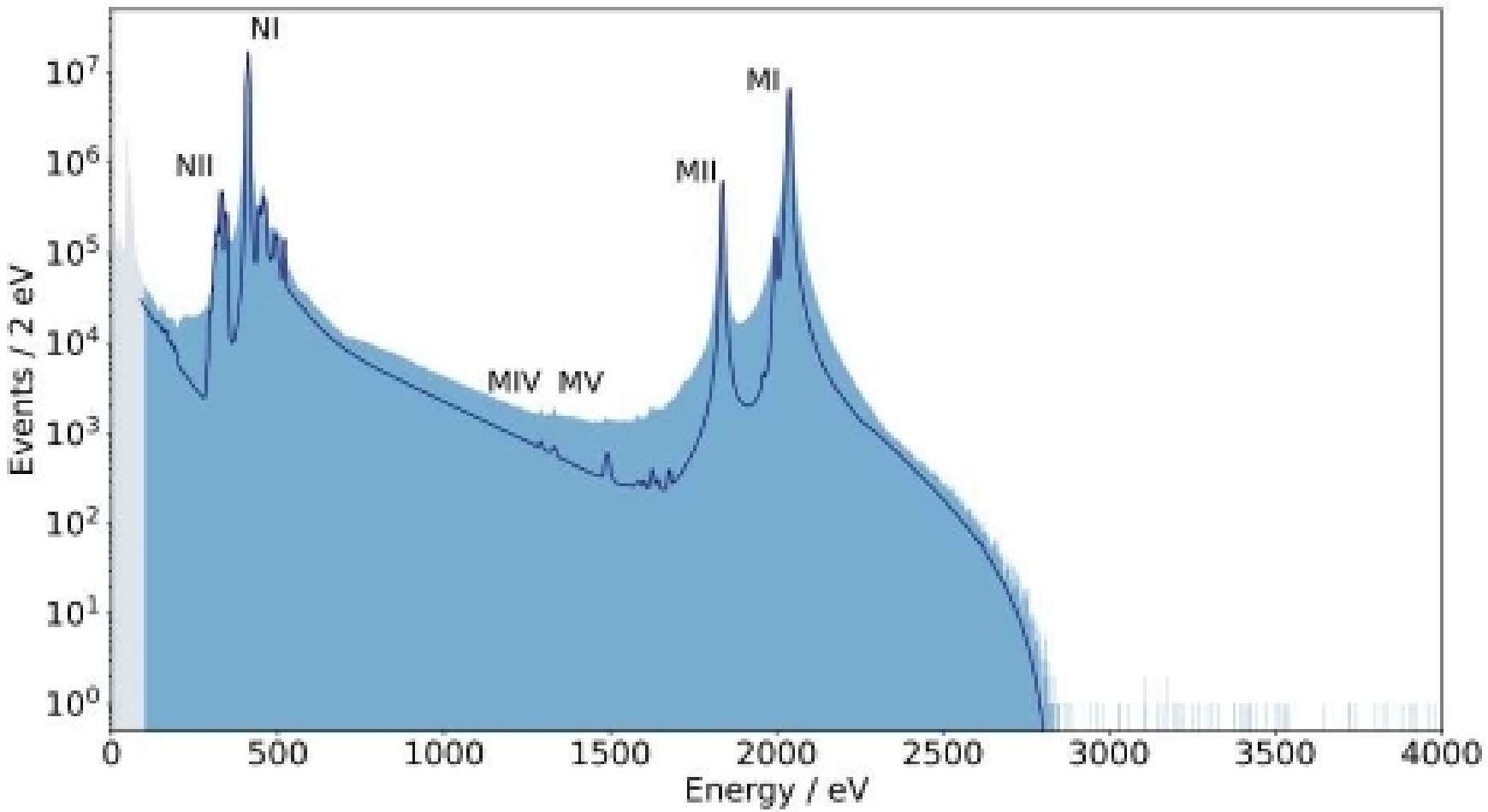

Figure: ECHo-1k experimental results [3]

Decay Rate

$$\lambda = \frac{G_\beta^2}{2\pi^3} \sum_x N_x C_x F_x S_x \tag{1}$$

$$F_x = \frac{\pi}{2} q_x^2 \beta_x^2 B_x \tag{2}$$

- $x = (n\kappa)$
- $k_x = |\kappa| \leq L$
- N_x - Relative occupation number
- p_x,q_x - Electron, neutrino momentum
- β_x - Coulomb amplitude
- B_x - The exchange and overlap correction factor
- S_x - The shake-up and shake-off correction factor

Decay Rate

$$
\begin{aligned}
C_x = & \left[M_L\left(k_x, k_\nu^{(1)}\right) + \left(\kappa_x/k_x\right) m_L\left(k_x, k_\nu^{(1)}\right) \right]^2 \\
& + \left[M_L\left(k_x, k_\nu^{(2)}\right) + \left(\kappa_x/k_x\right) m_L\left(k_x, k_\nu^{(2)}\right) \right]^2 \\
& + \left[M_{L+1}\left(k_x, k_\nu^{(2)}\right) + \left(\kappa_x/k_x\right) m_{L+1}\left(k_x, k_\nu^{(2)}\right) \right]^2 \\
& + \delta_{\Delta J,0} \left[M_0(1,1) + \left(\kappa_x/k_x\right) m_0(1,1) \right]^2
\end{aligned}
\tag{3}
$$

For (L-1)th unique forbidden transitions:

$$
C_x = \frac{(2L-2)!!}{(2L-1)!!} \left({}^A F^0_{LL-11} \right)^2 R^{2(L-1)} \frac{p_x^{2(k_x-1)} q_x^{2(L-k_x)}}{(2k_x-1)! \left\{2\left(L-k_x\right)+1\right\}!} \tag{4}
$$

For allowed transitions: $C_x = \delta_{\Delta J,0} \left({}^V F^0_{000} \right)^2 + \left({}^A F^0_{101} \right)^2$

More decay constant

$$
\begin{aligned}
k_\nu^{(1)} &= L - k_x + 1, \\
k_\nu^{(2)} &= L - k_x + 2.
\end{aligned}
\tag{5}
$$

$$
\begin{aligned}
&M_L\left(k_x, k_\nu^{(1)}\right) = K_L \left(p_x R\right)^{k_x - 1} \left(q_x R\right)^{k_\nu^{(1)} - 1} \times \\
&\left\{ -\left[(2L+1)/L\right]^{1/2} \ {}^{V}F^0_{LL-11} + \left(2k_x+1\right)^{-1/2} \alpha Z \ {}^{V}F^0_{LL0}\left(k_x, 1, 1, 1\right) \right. \\
&+ \left[\left(2k_x+1\right)^{-1} \left(2k_\nu^{(1)}+1\right)^{-1} q_x R \right] {}^{V}F^0_{LL0} - \\
&\left(2k_x+1\right)^{-1} \alpha Z \left[(L+1)/L\right]^{1/2} \ {}^{A}F^0_{LL1}\left(k_x, 1, 1, 1\right) \\
&\left. - \left[\left(2k_x+1\right)^{-1} W_x R + \left(2k_\nu^{(1)}+1\right)^{-1} q_x R \right] \left[(L+1)/L\right]^{1/2} \ {}^{A}F^0_{LL1} \right\}
\end{aligned}
\tag{6}
$$

More decay constant

$$m_L\left(k_x, k_\nu^{(1)}\right) = K_L\left(p_x R\right)^{k_x-1}\left(q_x R\right)^{k_\nu^{(1)}-1}\left(2k_x+1\right)^{-1} R$$
$$\left\{{}^V F_{LL0}^0 - \left[(L+1)/L\right]^{1/2\,A} F_{LL1}^0\right\},$$
$$M_L\left(k_x, k_\nu^{(2)}\right) = -\tilde{K}_L\left(p_x R\right)^{k_x-1}\left(q_x R\right)^{k_\nu^{(2)}-1}\sqrt{\frac{L+1}{\left(2k_x-1\right)\left(2k_\nu^{(2)}-1\right)}} \quad (7)$$
$$\left\{{}^V F_{LL0}^0 + \left(k_x - k_\nu^{(2)}\right)(L+1)^{-1}\left[(L+1)/L\right]^{1/2}\ {}^A F_{LL1}^0\right\},$$
$$M_{L+1}\left(k_x, k_\nu^{(2)}\right) = -\tilde{K}_L\left(p_x R\right)^{k_x-1}\left(q_x R\right)^{k_\nu^{(2)}-1}\ {}^A F_{(L+1)L1}^0.$$

$$K_L = (1/2)^{1/2}\left[(2L)!!/(2L+1)!!\right]^{1/2}\left[\left(2k_x-1\right)!\left(2k_\nu^{(1)}-1\right)!\right]^{-1/2}, \quad (8)$$
$$\tilde{K}_L = \left[(2L)!!/(2L+1)!!\right]^{1/2}\left[\left(2k_x-1\right)!\left(2k_\nu^{(2)}-1\right)!\right]^{-1/2}. \quad (9)$$

Form-factors and nuclear matrix elements

$$
\begin{aligned}
{}^{V}F^{N}_{KLs}\left(k_x,m,n,\rho\right) &= (-1)^{K-L}\ {}^{V}\mathfrak{M}^{N}_{KLs}\left(k_x,m,n,\rho\right),\\
{}^{A}F^{N}_{KLs}\left(k_x,m,n,\rho\right) &= (-1)^{K-L}\ g_A\ {}^{A}\mathfrak{M}^{N}_{KLs}\left(k_x,m,n,\rho\right),
\end{aligned}
\tag{10}
$$

$$
\begin{aligned}
{}^{V}F^{N}_{KLs} = {}^{V}F^{N}_{KLs}\left(k_x,m,n,0\right) &= (-1)^{K-L}\ {}^{V}\mathfrak{M}^{N}_{KLs}\left(k_x,m,n,0\right),\\
{}^{A}F^{N}_{KLs} = {}^{A}F^{N}_{KLs}\left(k_x,m,n,0\right) &= (-1)^{K-L}\ g_A\ {}^{A}\mathfrak{M}^{N}_{KLs}\left(k_x,m,n,0\right),
\end{aligned}
\tag{11}
$$

$$
(-1)^{J_f-M_f}\begin{pmatrix} J_f & K & J_i\\ -M_f & M & M_i\end{pmatrix}\left\{{}^{V}\mathfrak{M}^{N}_{KLs}\left(k_x,m,n,\rho\right)+g_A\ {}^{A}\mathfrak{M}^{N}_{KLs}\left(k_x,m,n,\rho\right)\right\}=\sqrt{\frac{4\pi}{2J_i+1}}\times
$$

$$
\iint\cdots\int\psi^{\dagger}_{f}\left(1,2,\ldots A;J_fM_f\pi_f\right)\times\sum_{j=1}^{A}\left\{\left(\frac{r}{R}\right)^{L*2N}I\left(k_x,m,n,\rho;r\right)\left(1+g_A\gamma_5\right)T^{M}_{KLs}\ \ t^{+}\right\}_{j}\times
$$

$$
\psi_i\left(1,2,\ldots A;J_iM_i\pi_i\right)d\tau_1d\tau_2\cdots d\tau_A.
\tag{12}
$$

Electronic wave function

$$\psi_{n\kappa m}(\vec{r}) = \begin{pmatrix} g_{n\kappa}(r)\Omega_{\kappa,m}(\hat{r}) \\ if_{n\kappa}(r)\Omega_{-\kappa,m}(\hat{r}) \end{pmatrix} \tag{13}$$

$$\begin{aligned} \left(\frac{d}{dr} + \frac{\kappa+1}{r}\right) g_{n\kappa}(r) &= (E_{n\kappa} - V(r) + m_e)\, f_{n\kappa}(r), \\ \left(\frac{d}{dr} - \frac{\kappa-1}{r}\right) f_{n\kappa}(r) &= -(E_{n\kappa} - V(r) - m_e)\, g_{n\kappa}(r). \end{aligned} \tag{14}$$

Coulomb Amplitudes

$$\begin{Bmatrix} g_{n\kappa}(r) \\ f_{n\kappa}(r) \end{Bmatrix} = \beta_{n\kappa} \frac{(p_{n\kappa}r)^{k-1}}{(2k-1)!!} \sum_{j=0}^{\infty} \begin{Bmatrix} a_j \\ b_j \end{Bmatrix} r^j \tag{15}$$

$$V_{\text{eff}} = \sum_{m=0}^{\infty} v_m r^m \tag{16}$$

DHFS Potential

$$V(r) \equiv V_{\text{DHFS}}(r) = V_{\text{nuc}}(r) + V_{\text{el}}(r) + V_{\text{ex}}(r) \tag{17}$$

A Fermi distribution for proton density is used to compute the nuclear potential.

$$\rho_p(r) = \frac{\rho_0}{1 + e^{(r-R_n)/a}}, \quad V_{\text{nuc}}(r) = -\alpha \int \frac{\rho_p(r')}{|\boldsymbol{r} - \boldsymbol{r}'|} d\boldsymbol{r}' \tag{18}$$

The electronic potential is computed from the electron density

$$\rho(r) = \sum_{n\kappa} \psi^{\dagger}_{n\kappa}(r)\psi_{n\kappa}(r), \quad V_{\text{el}}(r) = \alpha \int \frac{\rho(r')}{|r - r'|} dr' \tag{19}$$

The exchange potential is

$$V_{\text{ex}}(r) = \begin{cases} -\frac{3}{2}\alpha \left(\frac{3}{\pi}\right)^{1/3} [\rho(r)]^{1/3} & r < r_{\text{Latter}} \\ -\frac{\alpha(Z-N+1)}{r} - V_{\text{nuc}}(r) - V_{\text{el}}(r) & r \geq r_{\text{Latter}} \end{cases} \tag{20}$$

DHFS Potential

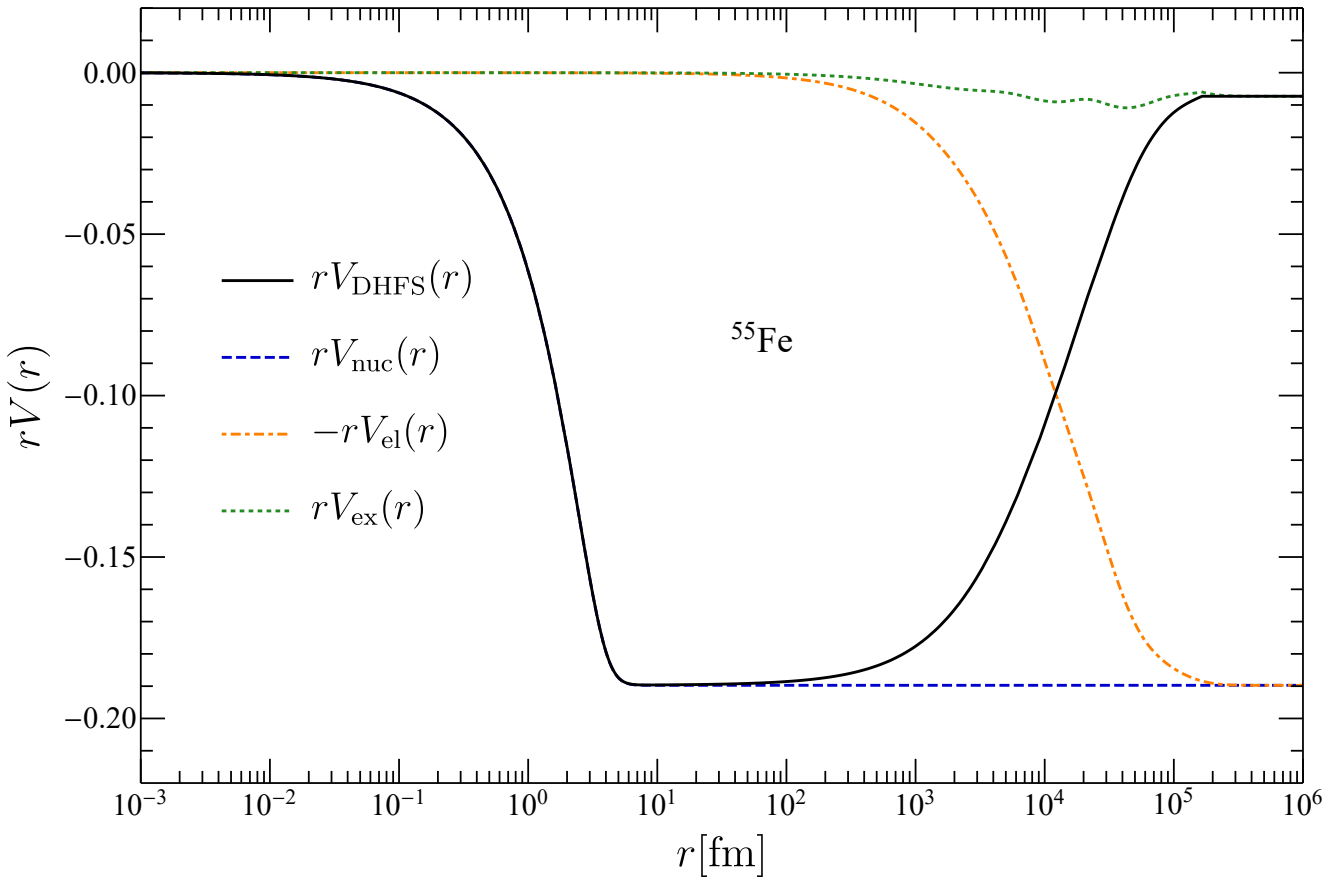

Figure: The DHFS potential (black) for neutral atom ^{55}Fe in ground state electronic configuration multiplied by the radius, along with its components.[4]

Binding energies

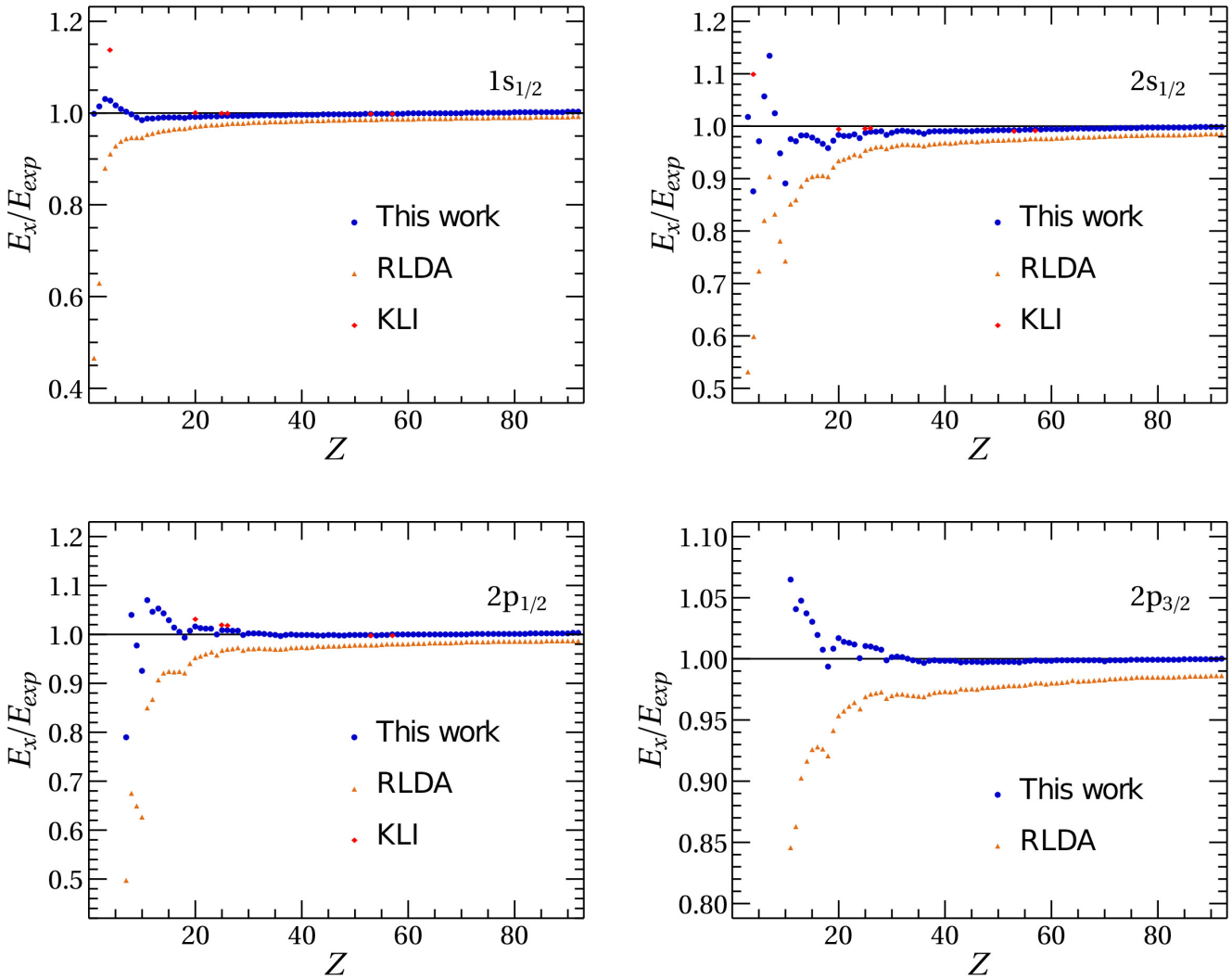

Figure: Comparison of theoretical binding energies with experimental values. [4]

The exchange and overlap correction

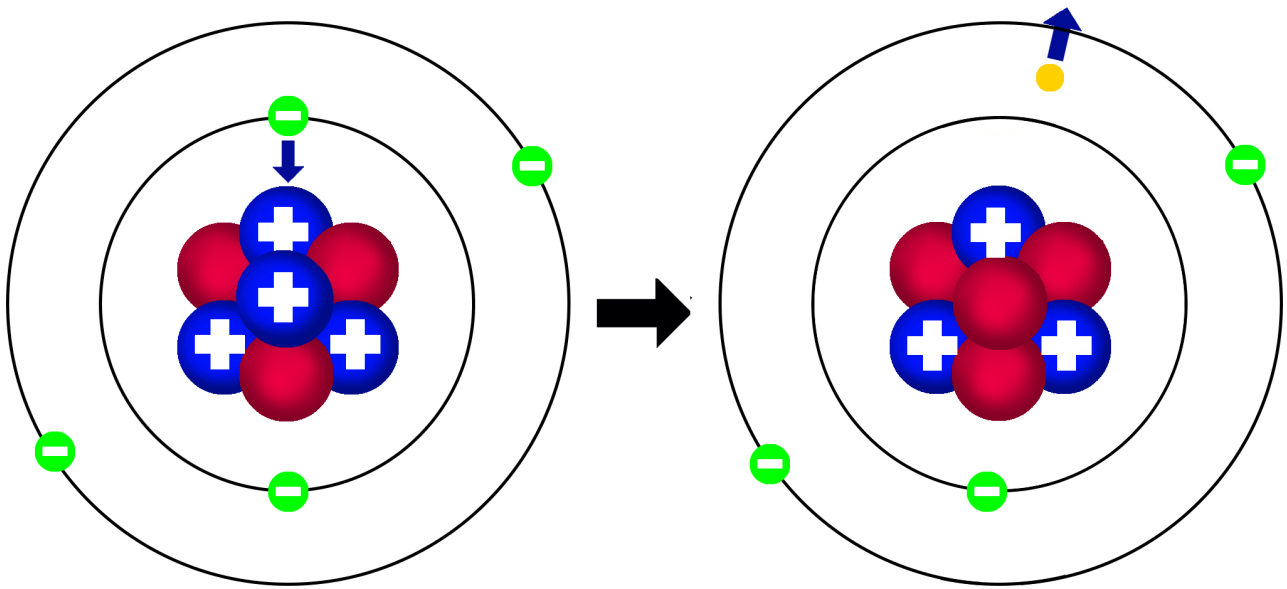

Figure: Electron Capture WITHOUT correction

The exchange and overlap correction

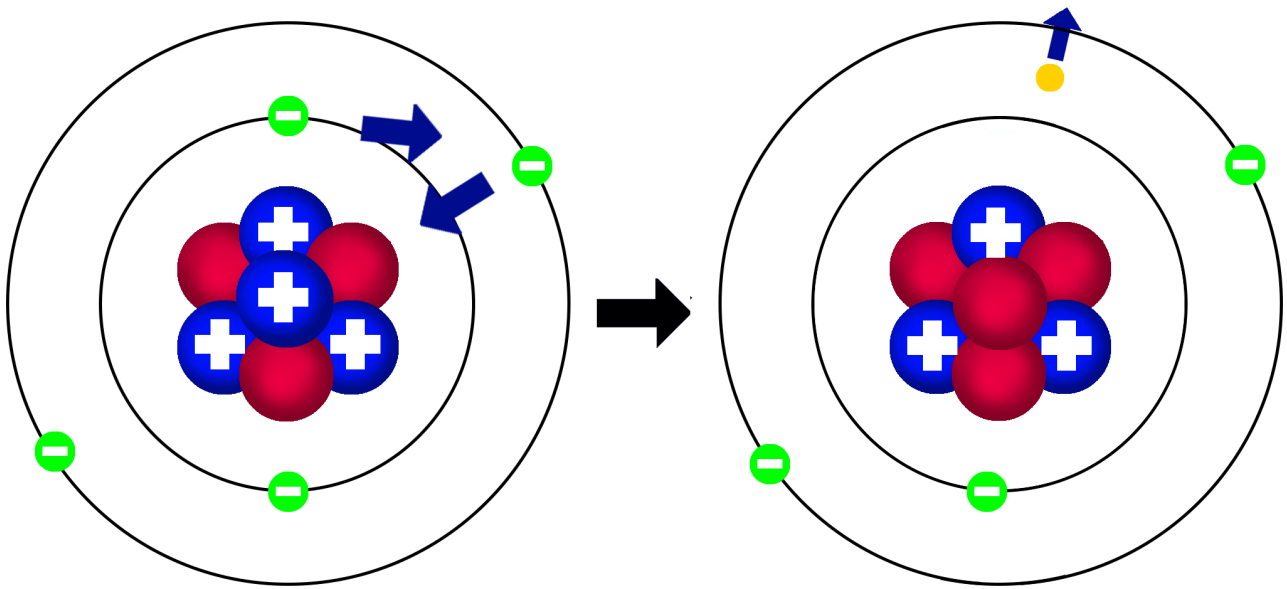

Figure: Electron Capture WITH correction

The exchange and overlap correction factor

The exchange and overlap correction takes into accounts the exchange between the captured electron and the measured position of the hole, and the imperfect overlap between initial and final wave function of the spectator electrons.

$$B_{n\kappa} = \left| \frac{b_{n\kappa}}{\beta_{n\kappa}} \right|^2 \tag{21}$$

$$b_{n\kappa} = \left[\prod_{m,\mu} \left\langle (m,\mu)' \middle| (m,\mu) \right\rangle^{n_{m\mu}} \right] \left\langle (n,\kappa)' \middle| (n,\kappa) \right\rangle^{-\frac{1}{2|\kappa|}} \times \left[\beta_{n\kappa} - \sum_{m \neq n} \beta_{m\kappa} \frac{\left\langle (m,\kappa)' \middle| (n,\kappa) \right\rangle}{\left\langle (m,\kappa)' \middle| (m,\kappa) \right\rangle} \right] \tag{22}$$

$B_{1-1} \approx 0.92 - 0.99$; $B_{n\kappa} \approx 0.8 - 2.1$

Shake-up and shake-off corrections

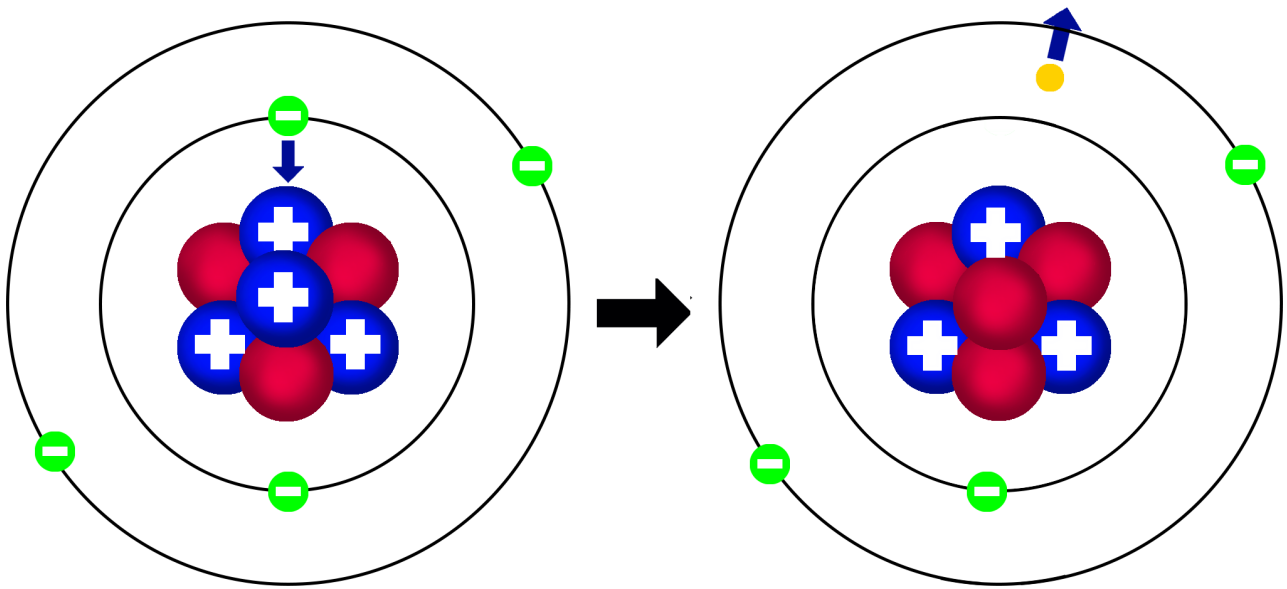

Figure: Electron Capture WITHOUT corrections

Shake-up and shake-off corrections

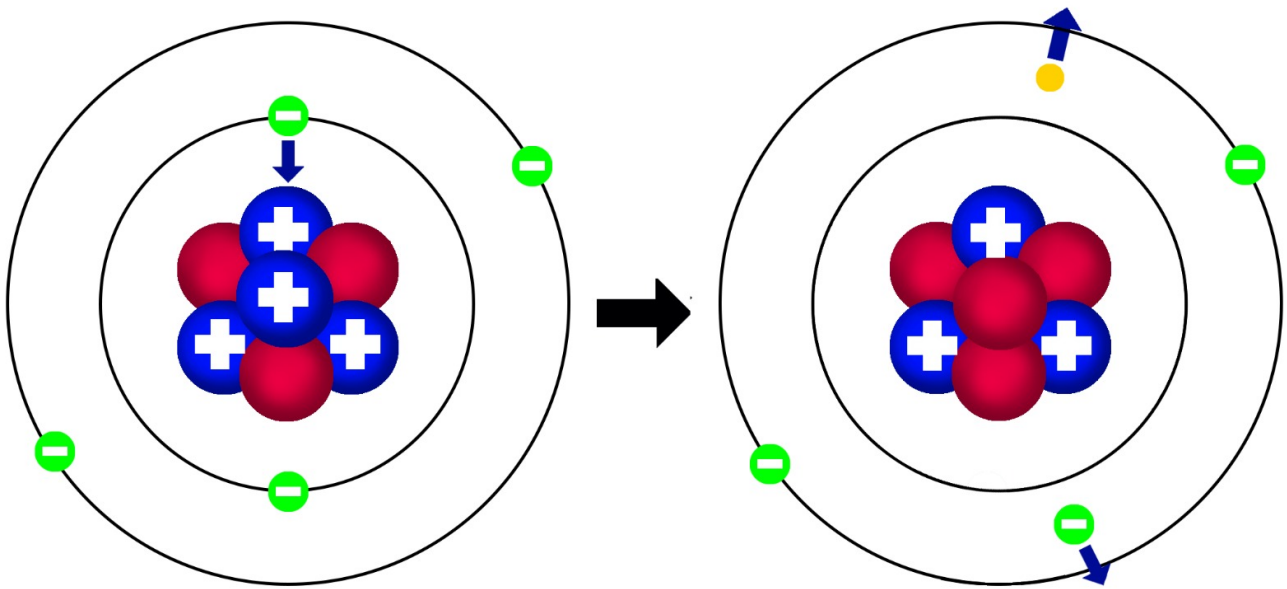

Figure: Electron Capture WITH shake-up and shake-off corrections

Shake-up and shake-off corrections

The shake-up and shake-off corrections takes into account the probability that an spectator electron is promoted to a upper vacant shell or is ejected in continuous.

$$S_{n\kappa} = 1 + \sum_{m,\mu} P_{m\mu} \tag{23}$$

$$\begin{aligned} P_{m\mu} = \quad & 1 - |\left\langle (m,\mu)' \middle| (m,\mu) \right\rangle|^{2n_{m\mu}} \\ & - \sum_{l \neq m} n'_{l\mu} n_{m\mu} |\left\langle (l,\mu)' \middle| (m,\mu) \right\rangle|^2 \end{aligned} \tag{24}$$

$S_{1-1} \approx 1 - 1.05$; $S_{n\kappa} \approx 1 - 1.21$

Energy conservation

Approximate formula:

$$M_i + m_e - |E_{n\kappa}| = M_f + R_\gamma + q_{n\kappa} \tag{25}$$

Refined formula:

$$\mathcal{M}_{gs}(A, Z) = \mathcal{M}_{n\kappa}(A, Z-1) + R_\gamma + q_{n\kappa} \tag{26}$$

$$\mathcal{M}_{gs}(A, Z) - \mathcal{M}_{gs}(A, Z-1) = \mathcal{M}_{n\kappa}(A, Z-1) - \mathcal{M}_{gs}(A, Z-1) + R_\gamma + q_{n\kappa} \tag{27}$$

$$\mathcal{M}_{gs}(A, Z) - \mathcal{M}_{gs}(A, Z-1) = |B_{gs}(Z-1)| - |B_{n\kappa}(Z-1)| + R_\gamma + q_{n\kappa} \tag{28}$$

$$R_{n\kappa} = |B_{gs}(Z-1)| - |B_{n\kappa}(Z-1)| \text{ - Released energy after EC} \tag{29}$$

$$\lambda_{n\kappa} \propto q_{n\kappa}^{2(L-k+1)} \text{(for unique transitions)} \tag{30}$$

Framework published in [4]

Atomic relaxation energy

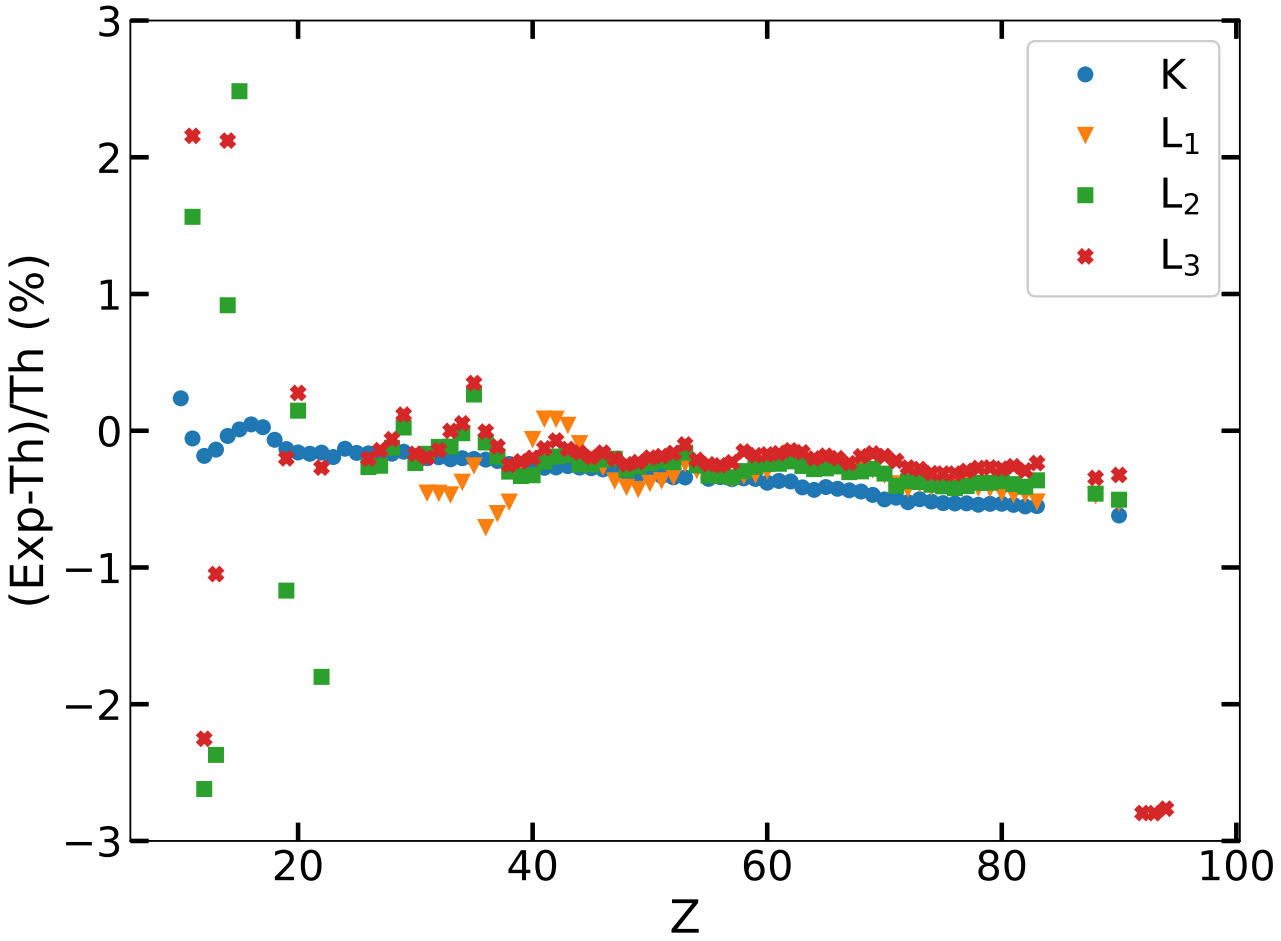

Figure: Comparison between theoretical and experimental atomic relaxation energy. [4]

Energy conservation

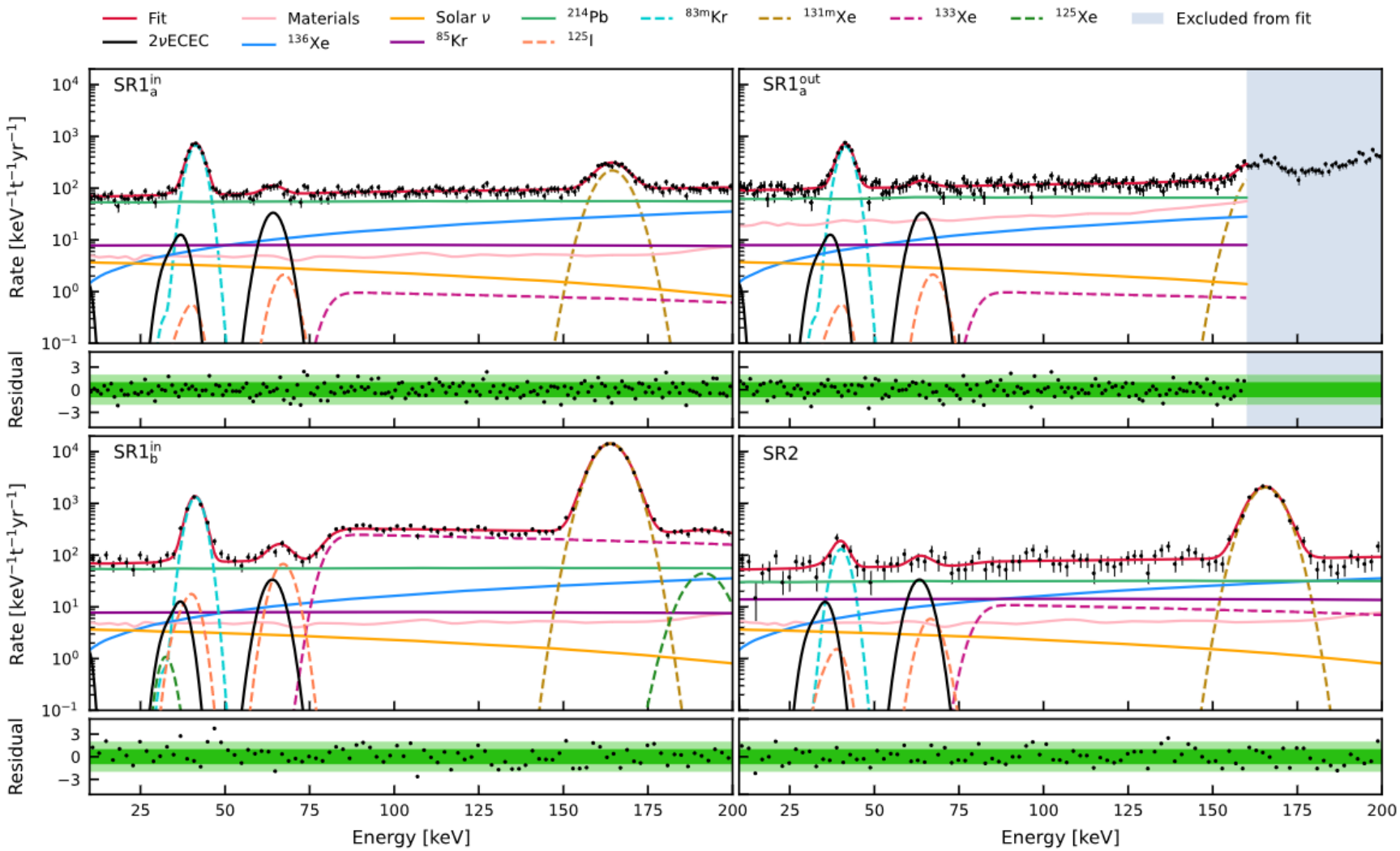

Figure: XENON1T Collaboration experimental results [2]

Comparison between formulas - K shell

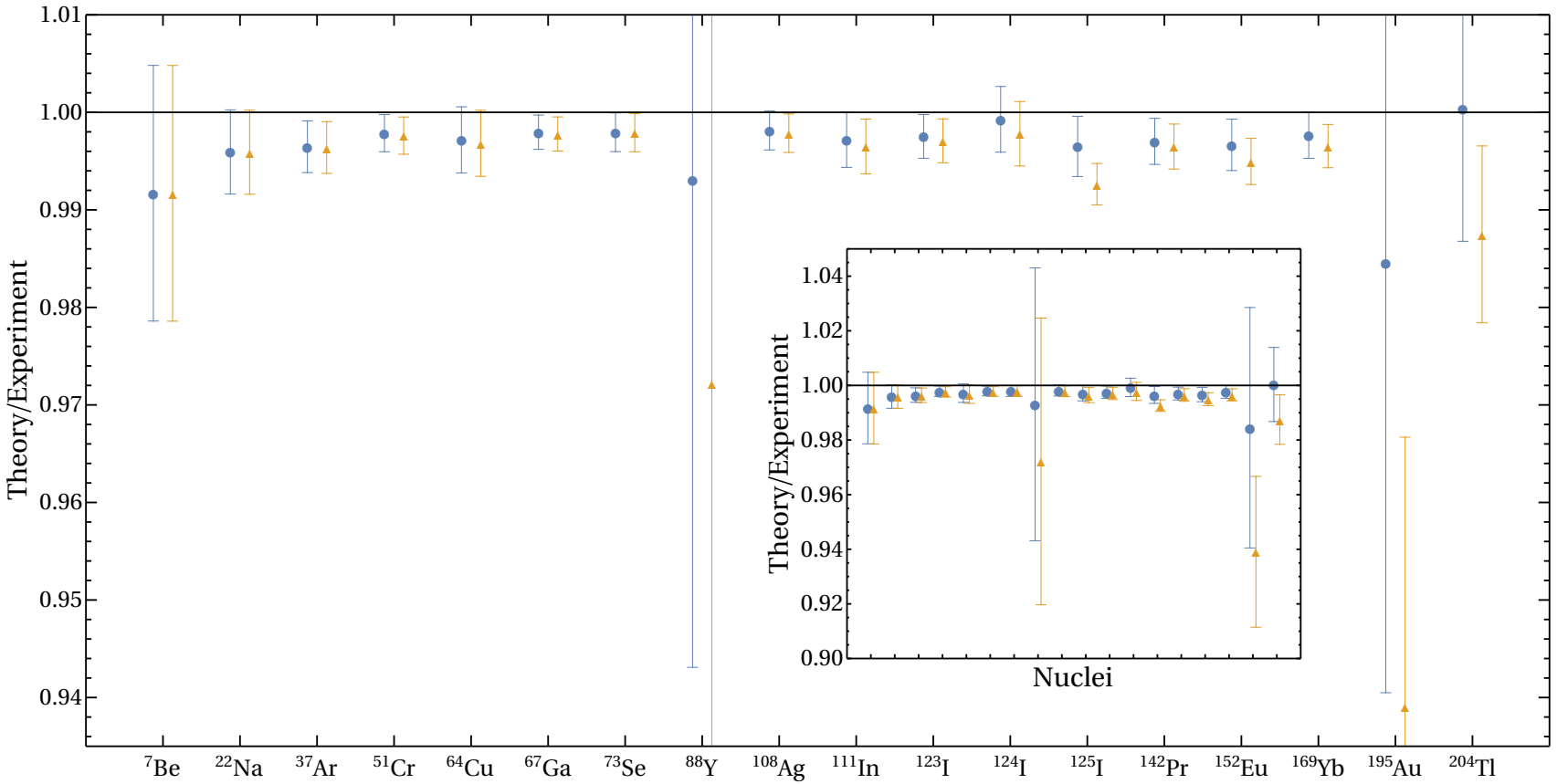

Figure: The ratio between the theoretical and experimental values for relative capture probability from the K shell considering both the approximate (orange triangle) and the refined (blue circle) formulas for energy conservation. [4]

Comparison between formulas - L shell

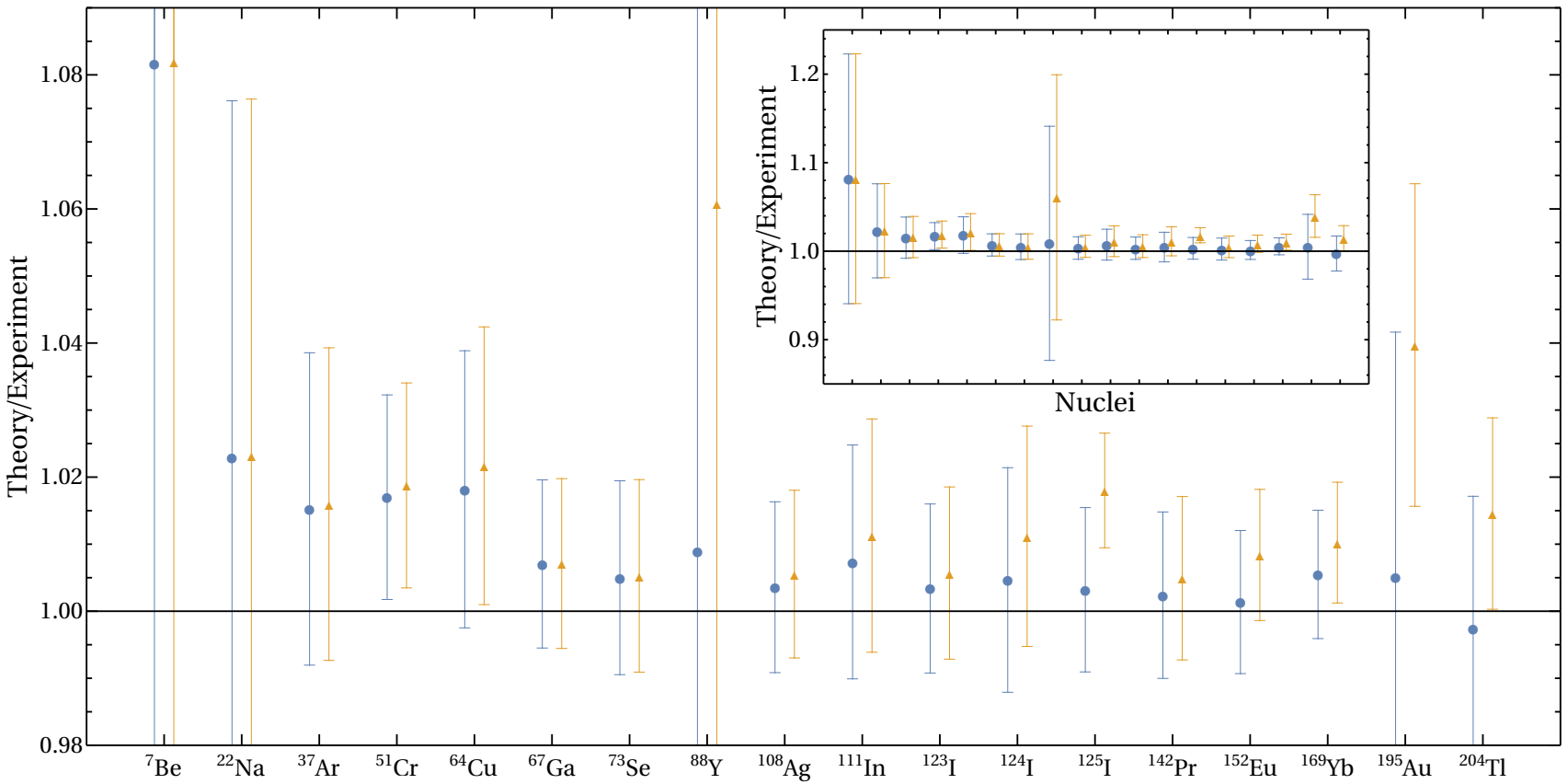

Figure: The ratio between the theoretical and experimental values for relative capture probability from the L shell considering both the approximate (orange triangle) and the refined (blue circle) formulas for energy conservation. [4]

EC ratios

Isotope	Q(keV)	R_γ(keV)	Type	Quantity	OW	RD
^{7}Be	861.89(7)	0	Allowed	λ_K/λ	0.90047(2)	0.908(12)
				λ_L/λ	0.09952(2)	0.092(12)
	861.89(7)	477.612(3)	Allowed	λ_K/λ	0.90046(5)	0.908(12)
				λ_L/λ	0.09954(5)	0.092(12)
^{64}Cu	1674.62(21)	1345.777(23)	Allowed	λ_K/λ	0.8815(2)	0.884(3)
				λ_L/λ	0.1008(2)	0.099(2)
				λ_M/λ	0.01714(3)	0.0162(5)
^{124}I	3159.6(19)	2335.03(1)	2nd UF	λ_K/λ	0.82040(273)	0.82099(43)
				λ_L/λ	0.14024(233)	0.13959(19)
				λ_M/λ	0.03099(54)	0.03135(15)
	3159.6(19)	2483.362(13)	1st UF	λ_K/λ	0.83148(215)	0.83184(41)
				λ_L/λ	0.13175(183)	0.13127(18)
				λ_M/λ	0.02891(43)	0.02928(14)
^{195}Au	226.8(10)	98.880(2)	1st UF	λ_K/λ	0.445(19)	0.452(6)
				λ_L/λ	0.400(14)	0.398(4)
				λ_{M+}/λ	0.1552(53)	0.1499(18)

Table: Comparison of our theoretical predictions and measured experimental data for electron capture ratios. This table is taken from [4].

L-shell dominance

Isotope	Q(keV)[5]	R_γ(keV)[6]		λ_K/λ	λ_L/λ	λ_M/λ	λ_{M+}/λ
^{127}Xe	662.33(546)	618.31(13)	OW	0.303(179)	0.520(125)	0.137(39)	0.177(50)
^{127}Xe	662.33(546)	618.31(13)	RD	0.310(80)	0.523(44)	0.137(12)	-
^{207}Bi	2397.41(266)	2339.92(0.8)	OW	0	0.638(8)	0.260(5)	0.362(7)
^{207}Bi	2397.41(266)	2339.92(0.8)	RD	0	0.651(6)	-	0.349(6)
^{236}Np	933.51(5043)	848.3(10)	OW	0	0.651(133)	0.245(79)	0.349(128)
^{236}Np	933.51(5043)	848.3(10)	RD	0	0.6(−)	-	0.4(−)

Table: Comparison of theoretical predictions and experimental results of electron capture probabilities for selected isotopes and transitions. This table is taken from [7].

EC in nuclear medicine

Isotope	Q(keV)[5]	R_γ(keV)[6]		λ_K/λ	λ_L/λ	$\lambda_M/\lambda \times 10^2$	$\lambda_N/\lambda \times 10^3$	$\lambda_O/\lambda \times 10^3$
^{67}Ga	1001.2(11)	0	This work	0.8818(3)	0.0995(3)	1.715(5)	1.504(5)	0
			RD	0.8836(15)	0.0989(12)	1.640(40)	-	
^{67}Ga	1001.2(11)	93.312(5)	This work	0.8816(3)	0.0997(3)	1.718(6)	1.507(5)	0
			RD	0.8834(15)	0.0991(12)	1.640(40)	-	
^{67}Ga	1001.2(11)	184.579(6)	This work	0.8814(4)	0.1000(3)	1.722(6)	1.510(6)	0
			RD	0.8832(15)	0.0993(12)	1.640(40)	-	
^{67}Ga	1001.2(11)	393.531(7)	This work	0.8806(5)	0.1005(4)	1.734(8)	1.521(8)	0
			RD	0.8824(15)	0.0999(12)	1.650(40)	-	
^{111}In	860(3)	416.72(3)	This work	0.8494(24)	0.11922(206)	2.520(46)	5.532(101)	0.609(11)
			RD	0.8518(2)	0.11835(13)	-	-	-
^{123}I	1228(3)	158.994(22)	This work	0.8513(10)	0.1166(8)	2.516(2)	5.913(45)	0.942(7)
			RD	0.8533(14)	0.1163(10)	2.48(5)	-	-
^{123}I	1228(3)	440.00(4)	This work	0.8489(13)	0.1185(11)	2.563(26)	6.027(61)	0.960(10)
			RD	0.8510(14)	0.1181(10)	2.53(5)	-	-
^{123}I	1228(3)	489.78(5)	This work	0.8482(14)	0.1190(12)	2.580(28)	6.057(66)	0.965(11)
			RD	0.8503(14)	0.1186(10)	2.54(5)	-	-
^{123}I	1228(3)	505.35(4)	This work	0.8480(14)	0.1191(13)	2.580(28)	6.067(68)	0.966(11)
			RD	0.8501(14)	0.1187(10)	2.54(5)	-	-
^{123}I	1228(3)	687.97(3)	This work	0.8444(20)	0.1219(17)	2.649(40)	6.233(94)	0.993(15)
			RD	0.8464(14)	0.1216(10)	2.62(5)	-	-
^{123}I	1228(3)	783.62(3)	This work	0.8412(25)	0.1243(21)	2.709(49)	6.380(117)	1.017(19)
			RD	0.8436(14)	0.1237(10)	2.67(5)	-	-

Table: Comparison theoretical and experimental values of relative capture probabilities for nuclei of interest in nuclear medicine. This table is taken from [4]

EC as a tool for neutrino mass determination

We consider $m_\nu \neq 0$ eV and take into account $\Gamma_x$the Breit-Wigner resonances centered at R_x for allowed and UF transitions:

$$\rho(E) = \frac{G_\beta^2}{(2\pi)^2} \sum_x N_x C_x \beta_x^2 B_x S_x q_x E_{\nu x} \frac{\Gamma_x/(2\pi)}{(E - R_x)^2 + \Gamma_x^2/4} \tag{31}$$

with

$$R_x = |B_{gs}(Z-1)| - |B_x(Z-1)| \tag{32}$$

Normalized distributions of released energy for ^{95}Tc

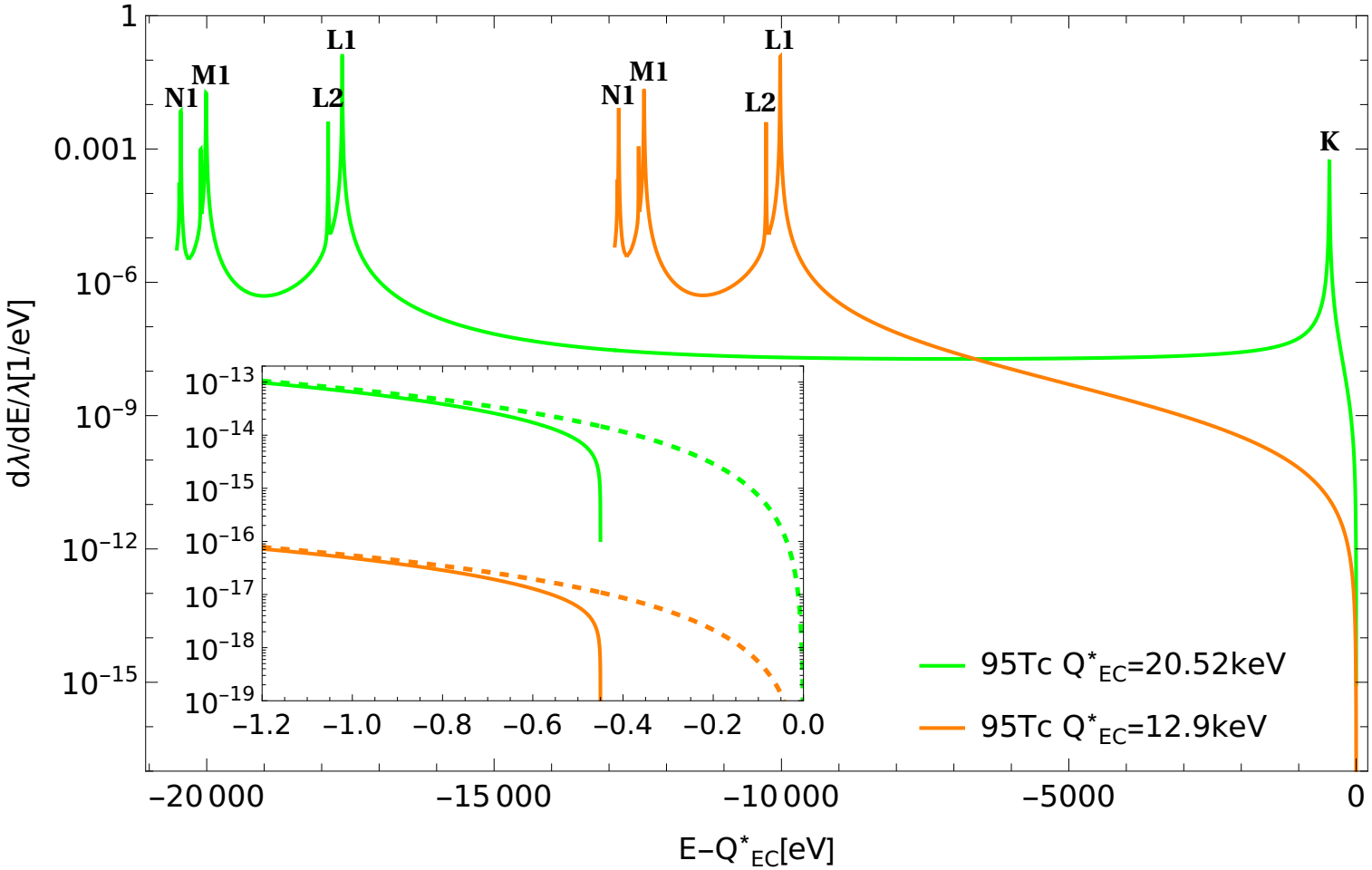

Figure: Normalized distributions of released energy in the EC decay of ^{95}Tc in the transitions to the two excited states of ^{95}Mo[8]

Comparison of ^{95}Tc with ^{163}Ho

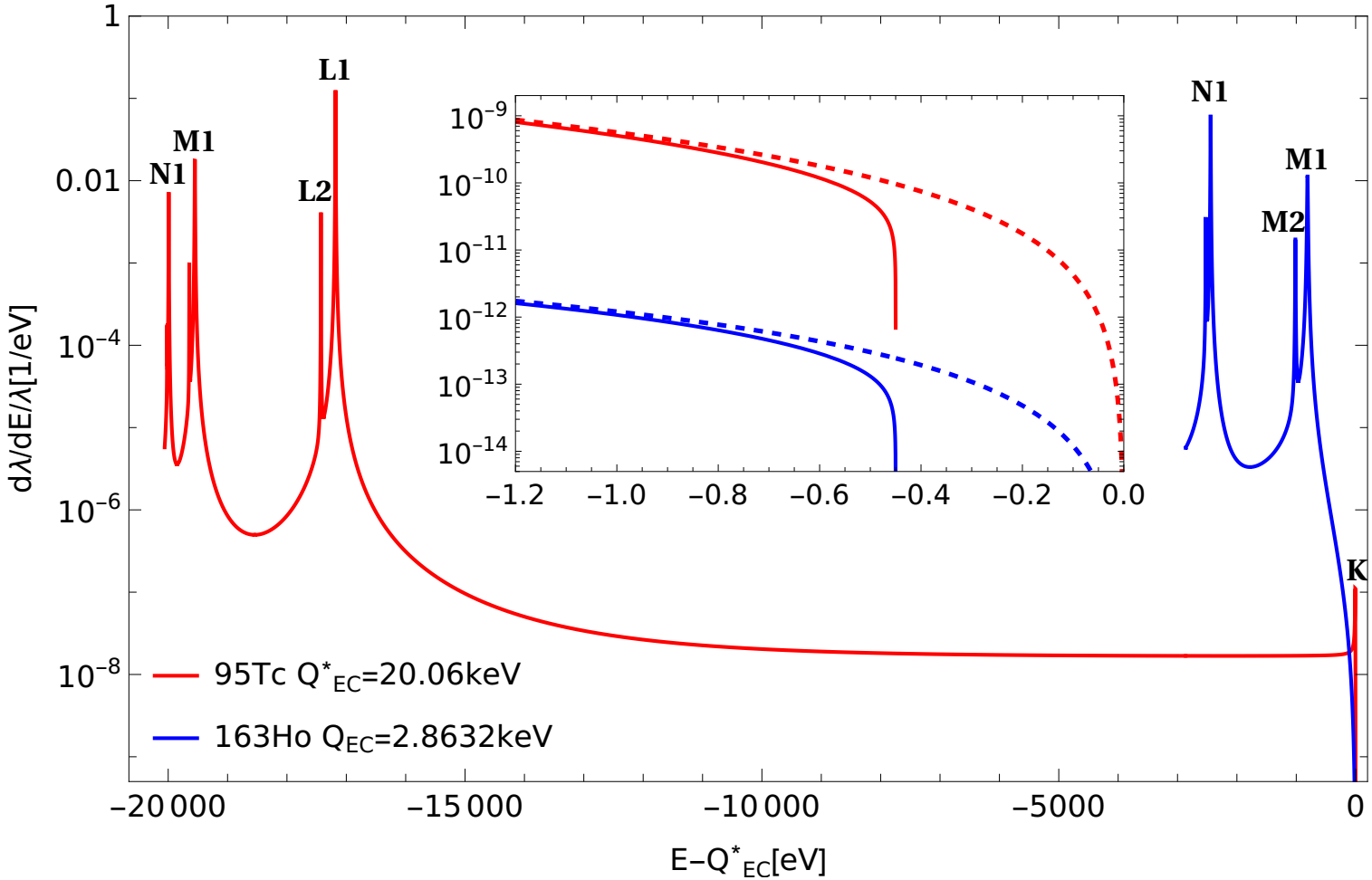

Figure: Normalized distributions of released energy in the EC decay of ^{95}Tc with Q^*_{EC} within 1σ range; and of ^{163}Ho[8]

Comparison of ^{97}Tc with ^{163}Ho

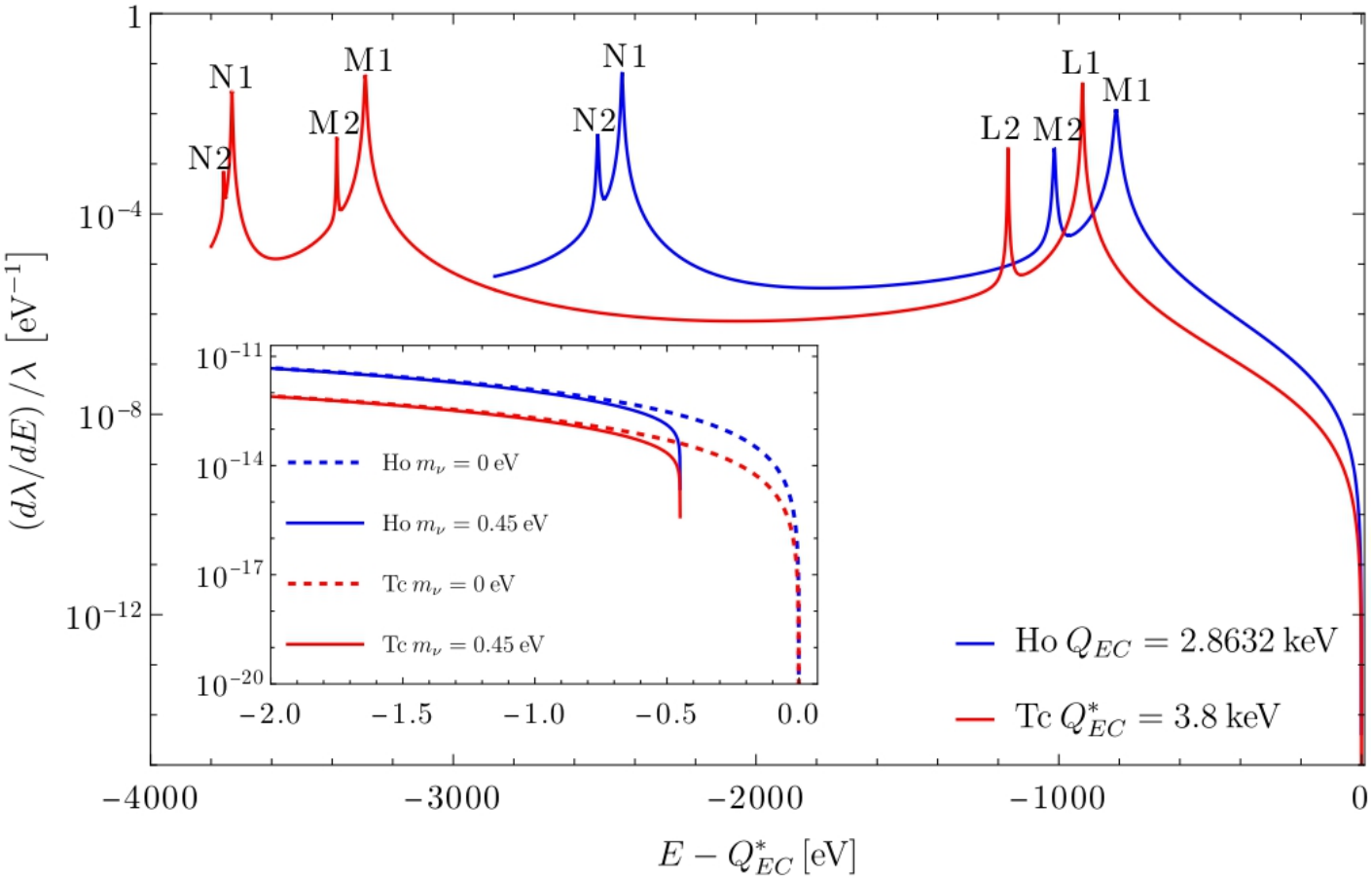

Figure: Normalized distributions of released energy in the EC decay of ^{97}Tc, assuming allowed transition type in comparison with ^{163}Ho.[9]

Statistical approach for ^{97}Tc

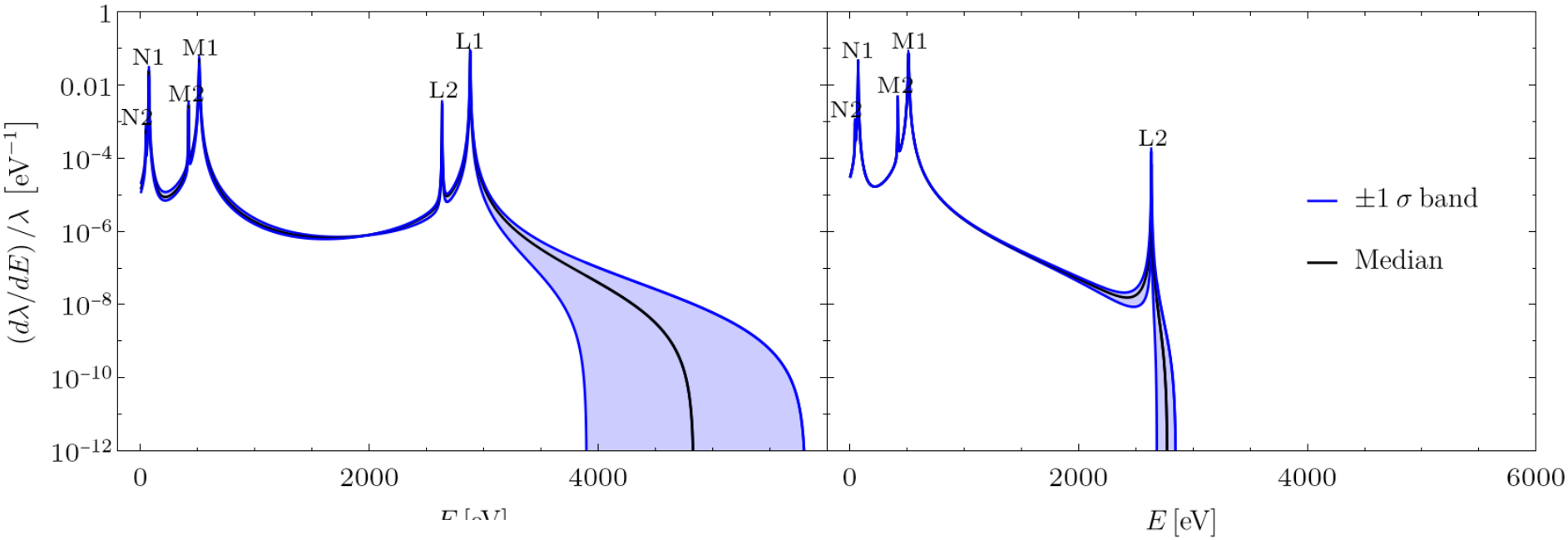

Figure: Normalized distributions of released energy as a function of E in the statistical approach for ^{97}Tc with Q^*_{EC} of 4.8(10) keV.[9]

Comparison of ^{113}Sn with ^{163}Ho

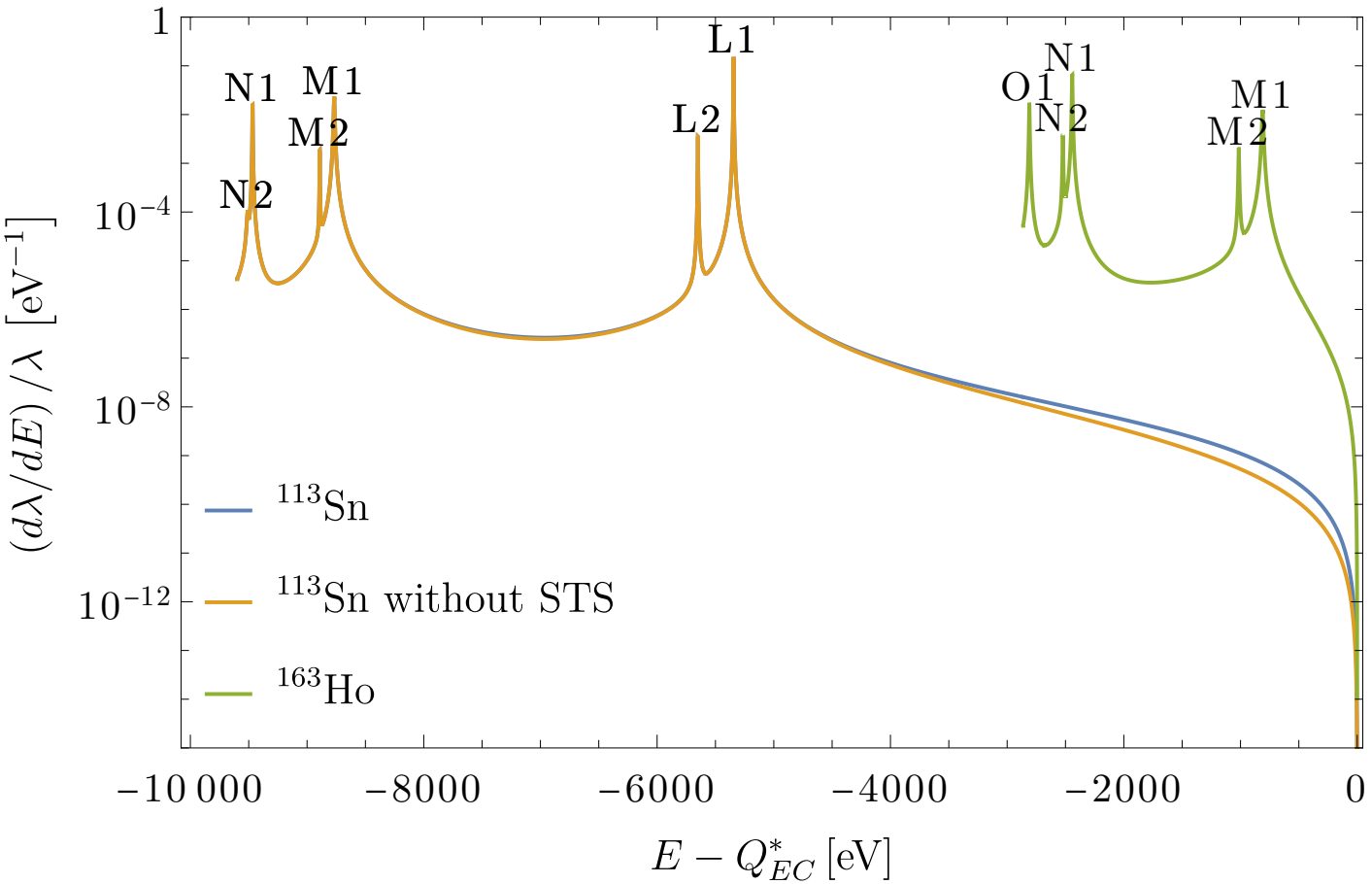

Figure: Normalized distributions of released energy in the EC decay of ^{113}Sn, as functions of $E - Q^*_{\mathrm{EC}}$, assuming allowed transition type in comparison with ^{163}Ho.

To be published...

Comparison of ^{113}Sn with ^{163}Ho - ZOOM

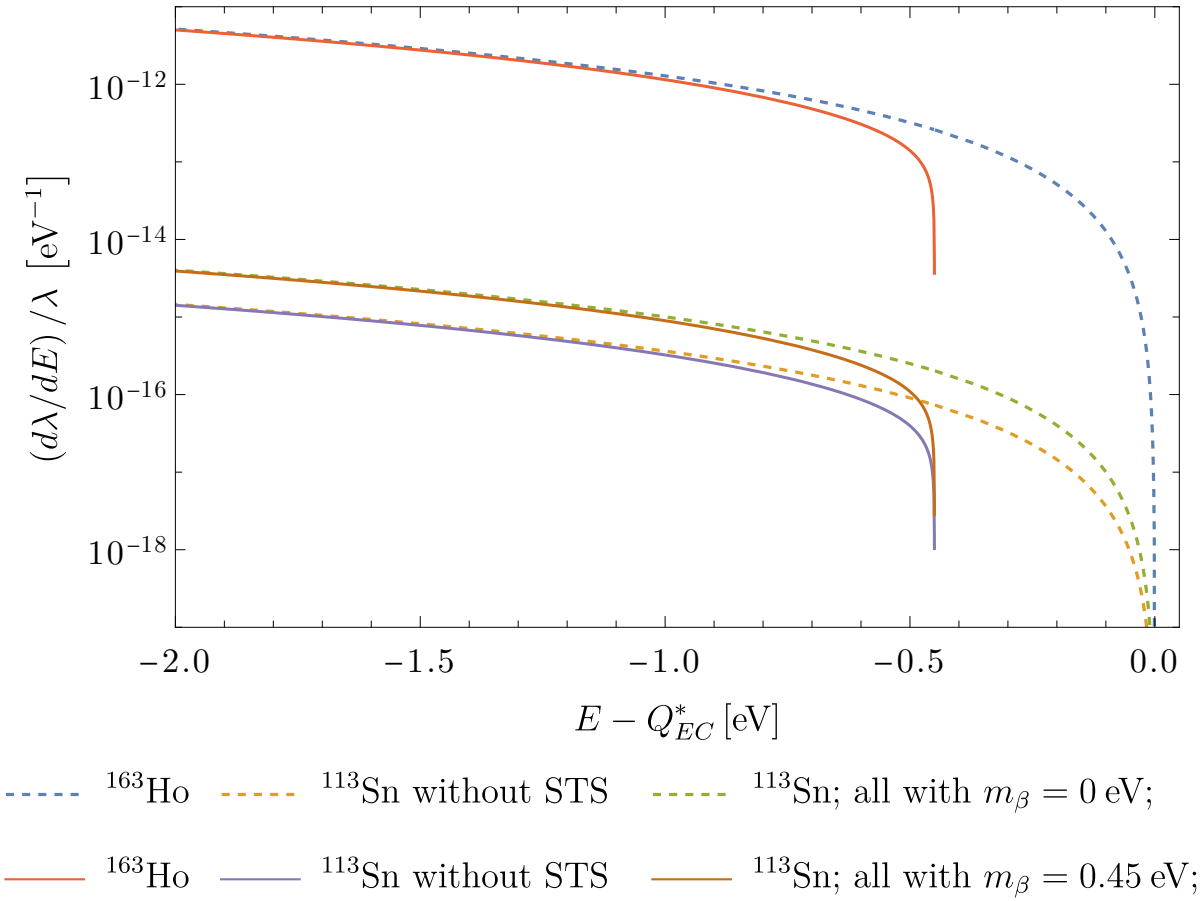

Figure: Zoom of the endpoint for the normalized distributions of released energy in the EC decay of ^{113}Sn in comparison with ^{163}Ho.

To be published...

Comparison of ^{148}Eu with ^{163}Ho

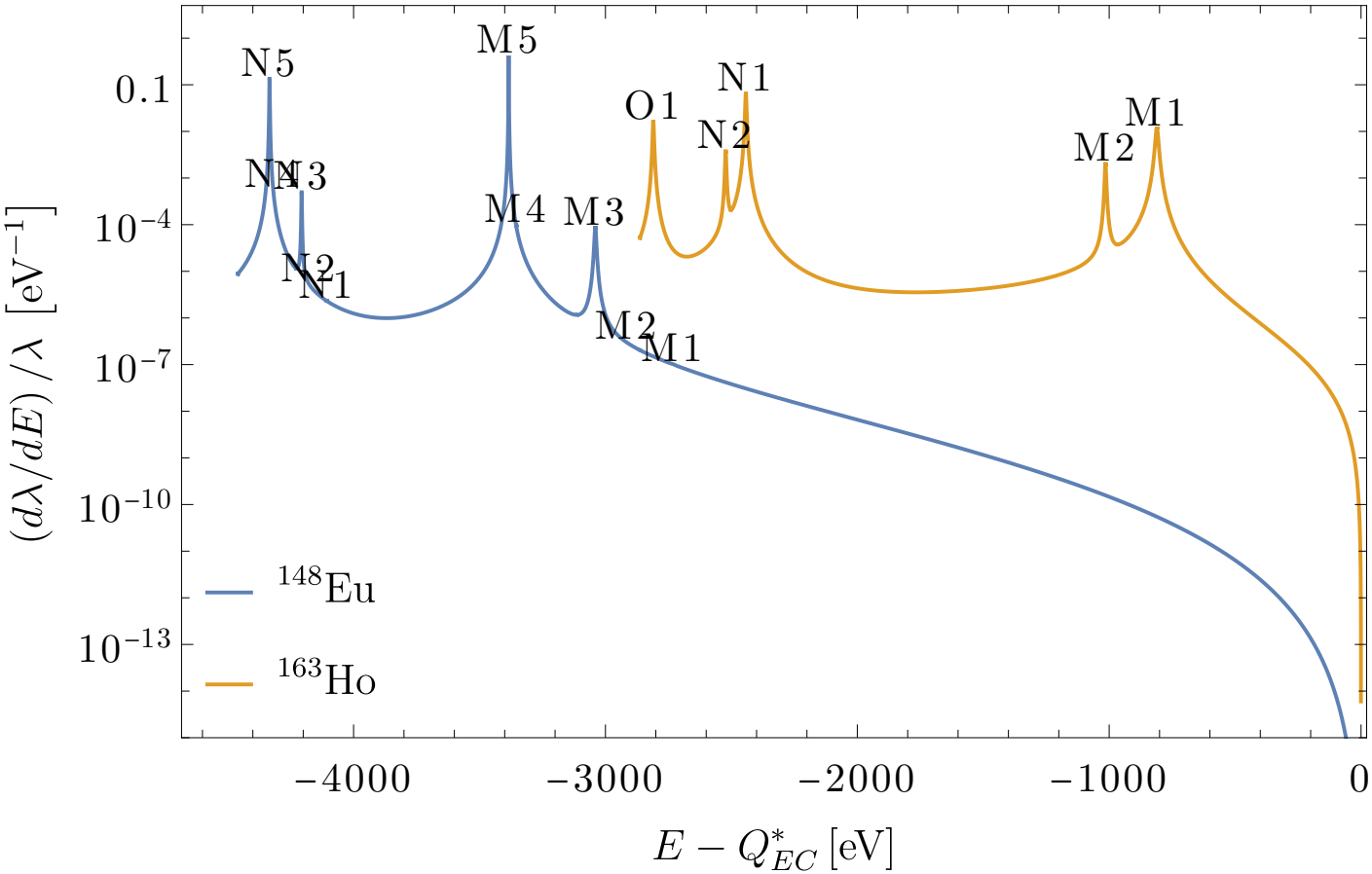

Figure: Normalized distributions of released energy in the EC decay of ^{148}Eu - 3rd UF, as functions of $E - Q^*_{\mathrm{EC}}$, in comparison with ^{163}Ho.

Work in progress

Half-life time predictions

Table: Theoretical predictions for partial half-life time for the EC decay of ^{95}Tc.[8]

Q^*_{EC} (keV)	interaction	M_{GT}	Total (10^3yr)	K (10^7yr)	L1 (10^4yr)	L2 (10^5yr)	M1 (10^4yr)
20.52(61)	jj45pna	−0.00696	877	20.0	117	708	640
	jj45pnb	-0.016533	155	3.55	20.8	125	81.6
	glekpn	0.0070667	850	19.4	114	587	446
12.9(10)	jj45pna	−0.02412	173	-	24.1	143	79.7
	jj45pnb	-0.0198667	255	-	35.6	210	117
	glekpn	0.2296	1.9	-	0.266	1.57	0.880

Q^*_{EC} (keV)	Final J	Total (yr)	L1 (yr)	L2 (yr)	L3 (10^9 yr)	M1 (yr)	M2 (yr)
9.60	3/2	33.56	59.60	2327.62	-	105.54	4158.28
9.60	1/2	238.08	422.75	16510.2	-	748.59	29495.3
14.97	5/2	4.04×10^9	7.15×10^{11}	2.79×10^{13}	5.85	1.12×10^{12}	4.40×10^{13}

Table: Computed half-lives for the electron capture decay of ^{113}Sn to the excited states of ^{113}In . The shell-model interaction used is jj45pnb. To be published.

Half-life time predictions

Table: Theoretical predictions for ^{97}Tc assuming L1 energetically available [9]

Type	Total	L1	L2	M1	M2	N1	N2	O1	
	(10^4)	(10^4)	(10^7)	(10^4)	(10^6)	(10^5)	(10^7)	(10^6)	
allowed	$19^{+17}_{-0.7}$	46^{+120}_{-26}	$2.2^{+5.0}_{-1.2}$	47^{+32}_{-17}	26^{+18}_{-10}	20^{+12}_{-7}	13^{+8}_{-4}	42^{+25}_{-15}	
	Total	L1	L2	L3	M1	M2	M3	M4	M5
2nd	(10^{16})	(10^{23})	(10^{24})	(10^{18})	(10^{21})	(10^{23})	(10^{18})	(10^{20})	(10^{16})
UF	$11^{+6.1}_{-3.4}$	$1.0^{+50}_{-0.92}$	$3.1^{+84}_{-2.7}$	$5.3^{+38}_{-4.0}$	$4.4^{+15}_{-3.1}$	$2.3^{+7.2}_{-1.6}$	$2.0^{+3.1}_{-1.1}$	$11^{+17}_{-6.2}$	$11^{+6.2}_{-3.4}$
	Total	L1	L2	L3	M1	M2	M3	M4	M5
4th	(10^{21})	(10^{28})	(10^{30})	(10^{24})	(10^{26})	(10^{28})	(10^{23})	(10^{25})	(10^{21})
NUF	$10^{+10}_{-3.6}$	$5.7^{+1066}_{-5.5}$	$1.4^{+116}_{-1.3}$	$2.6^{+58}_{-2.3}$	$5.0^{+31}_{-4.0}$	$2.5^{+1.4}_{-2.0}$	$2.6^{+8.4}_{-1.8}$	$14^{+42}_{-1.0}$	$7.2^{+11}_{-3.9}$

Table: Theoretical predictions for ^{97}Tc assuming L1 energetically unavailable [9]

Type	Total	L2	M1	M2	N1	N2	O1	
	(10^4)	(10^9)	(10^5)	(10^6)	(10^5)	(10^7)	(10^7)	
allowed	93^{+7}_{-6}	$5.7^{+40}_{-3.4}$	$16.9^{+5}_{-3.4}$	91^{+27}_{-18}	60^{+18}_{-12}	38^{+11}_{-8}	$12.7^{+4}_{-2.5}$	
	Total	L2	L3	M1	M2	M3	M4	M5
2nd	(10^{16})	(10^{31})	(10^{22})	(10^{21})	(10^{23})	(10^{18})	(10^{21})	(10^{16})
UF	$33^{+2.5}_{-1.9}$	$4.9^{+2326}_{-4.5}$	$4.1^{+21}_{-2.7}$	215^{+59}_{-38}	98^{+26}_{-17}	$24^{+4.0}_{-2.8}$	$12^{+1.9}_{-1.4}$	$35^{+2.6}_{-2.0}$
	Total	L2	L3	M1	M2	M3	M4	M5
4th	(10^{21})	(10^{39})	(10^{30})	(10^{28})	(10^{29})	(10^{23})	(10^{26})	(10^{21})
NUF	$74^{+11}_{-8.3}$	$6.1^{+25320}_{-5.9}$	$1.9^{+26}_{-1.5}$	$9^{+3.4}_{-2.1}$	$38^{+14}_{-8.7}$	110^{+29}_{-19}	$51^{+12}_{-8.4}$	$78^{+12}_{-8.8}$

Conclusion and outlook

- Relative capture probability, half-life times and other intermediate quantities were calculated
- We considered the exchange and overlap corrections and the shake-up and shake-off corrections
- We improved the way the energy conservation was taken into account
- We implemented the error propagation through pseudo-experiments
- We plotted the distribution of released energy for both ^{95}Tc, ^{97}Tc, and ^{113}Sn in comparison with ^{163}Ho

E. Bezak, B. Q. Lee, T. Kibédi, A. E. Stuchbery, and K. A. Robertson, "Atomic radiations in the decay of medical radioisotopes: A physics perspective," *Computational and Mathematical Methods in Medicine*, vol. 2012, p. 651475, 2012. [Online]. Available: https://doi.org/10.1155/2012/651475

E. Aprile, K. Abe, F. Agostini, S. Ahmed Maouloud, M. Alfonsi, L. Althueser, B. Andrieu, E. Angelino, J. R. Angevaare, V. C. Antochi, D. Antón Martin, F. Arneodo, L. Baudis, A. L. Baxter, L. Bellagamba, R. Biondi, A. Bismark, A. Brown, S. Bruenner, G. Bruno, R. Budnik, C. Cai, C. Capelli, J. M. R. Cardoso, D. Cichon, M. Clark, A. P. Colijn, J. Conrad, J. J. Cuenca-García, J. P. Cussonneau, V. D'Andrea, M. P. Decowski, P. Di Gangi, S. Di Pede, A. Di Giovanni, R. Di Stefano, S. Diglio, K. Eitel, A. Elykov, S. Farrell, A. D. Ferella, H. Fischer, W. Fulgione, P. Gaemers, R. Gaior, A. Gallo Rosso, M. Galloway, F. Gao, R. Glade-Beucke, L. Grandi, J. Grigat, M. Guida, A. Higuera, C. Hils, L. Hoetzsch, J. Howlett, M. Iacovacci, Y. Itow, J. Jakob, F. Joerg, A. Joy, N. Kato,

M. Kara, P. Kavrigin, S. Kazama, M. Kobayashi, G. Koltman, A. Kopec, H. Landsman, R. F. Lang, L. Levinson, I. Li, S. Li, S. Liang, S. Lindemann, M. Lindner, K. Liu, J. Loizeau, F. Lombardi, J. Long, J. A. M. Lopes, Y. Ma, C. Macolino, J. Mahlstedt, A. Mancuso, L. Manenti, A. Manfredini, F. Marignetti, T. Marrodán Undagoitia, K. Martens, J. Masbou, D. Masson, E. Masson, S. Mastroianni, M. Messina, K. Miuchi, K. Mizukoshi, A. Molinario, S. Moriyama, K. Morå, Y. Mosbacher, M. Murra, J. Müller, K. Ni, U. Oberlack, B. Paetsch, J. Palacio, R. Peres, J. Pienaar, M. Pierre, V. Pizzella, G. Plante, J. Qi, J. Qin, D. Ramírez García, S. Reichard, A. Rocchetti, N. Rupp, L. Sanchez, J. M. F. dos Santos, I. Sarnoff, G. Sartorelli, J. Schreiner, D. Schulte, P. Schulte, H. Schulze Eißing, M. Schumann, L. Scotto Lavina, M. Selvi, F. Semeria, P. Shagin, S. Shi, E. Shockley, M. Silva, H. Simgen, A. Takeda, P.-L. Tan, A. Terliuk, D. Thers, F. Toschi, G. Trinchero, C. Tunnell, F. Tönnies, K. Valerius, G. Volta, Y. Wei, C. Weinheimer, M. Weiss, D. Wenz, C. Wittweg, T. Wolf, Z. Xu, M. Yamashita, L. Yang, J. Ye, L. Yuan, G. Zavattini, S. Zerbo,

M. Zhong, and T. Zhu, "Double-weak decays of ^{124}Xe and ^{136}Xe in the xenon1t and xenonnt experiments," *Phys. Rev. C*, vol. 106, p. 024328, Aug 2022. [Online]. Available: https://link.aps.org/doi/10.1103/PhysRevC.106.024328

F. Adam, F. Ahrens, L. E. A. Perez, M. Balzer, A. Barth, D. Behrend-Uriarte, S. Berndt, K. Blaum, F. W. H. Böhm, M. Braß, L. Calza, K. Chrysalidis, M. Door, H. Dorrer, C. E. Düllmann, K. Eberhardt, S. Eliseev, C. Enss, P. Filianin, A. Fleischmann, R. Gartmann, L. Gastaldo, M. Griedel, A. Göggelmann, R. Hammann, R. Hasse, M. W. Haverkort, S. Heinze, D. Hengstler, R. Jeske, J. Jochum, K. Johnston, N. Karcher, S. Kempf, T. Kieck, U. Köster, N. Kovac, N. Kneip, K. Kromer, F. Mantegazzini, B. A. Marsh, M. Merstof, T. Muscheid, M. Neidig, Y. N. Novikov, R. Pandey, A. Reifenberger, D. Richter, A. Rischka, S. Rothe, O. Sander, R. X. Schüssler, S. Scholl, C. Schweiger, C. Velte, M. Weber, M. Wegner, K. Wendt, and T. Wickenhäuser, "Improved limit on the effective

electron neutrino mass with the echo-1k experiment," 2025. [Online]. Available: https://arxiv.org/abs/2509.03423


V. A. Sevestrean, O. Nitescu, S. Ghinescu, and S. Stoica, "Self-consistent calculations for atomic electron capture," *PHYSICAL REVIEW A*, vol. 108, no. 1, JUL 17 2023.


M. Wang, W. Huang, F. Kondev, G. Audi, and S. Naimi, "The ame 2020 atomic mass evaluation (ii). tables, graphs and references*," *Chinese Physics C*, vol. 45, no. 3, p. 030003, mar 2021. [Online]. Available: https://dx.doi.org/10.1088/1674-1137/abddaf


"Livechart - table of nuclides - nuclear structure and decay data," *Livechart - table of nuclides - nuclear structure and decay data*. [Online]. Available: https://www-nds.iaea.org/relnsd/vcharthtml/VChartHTML.html

V. A. Sevestrean, O. Nițescu, S. Ghinescu, and S. Stoica, "L-shell capture dominance in 127 xe, 207 bi and 236 np," *AIP Conference Proceedings*, vol. 3138, no. 1, p. 020017, 09 2024. [Online]. Available: https://doi.org/10.1063/5.0214587

Z. Ge, T. Eronen, V. A. Sevestrean, O. Nitescu, S. Stoica, M. Ramalho, J. Suhonen, A. de Roubin, D. Nesterenko, A. Kankainen, P. Ascher, S. A. S. Andres, O. Beliuskina, P. Delahaye, M. Flayol, M. Gerbaux, S. Grevy, M. Hukkanen, A. Jaries, A. Jokinen, A. Husson, D. Kahl, J. Kostensalo, J. Kotila, I. Moore, S. Nikas, M. Stryjczyk, and V. Virtanen, "High-precision measurements of the atomic mass and electron-capture decay q value of 95 tc," *PHYSICS LETTERS B*, vol. 859, DEC 2024.

Z. Ge, T. Eronen, V. A. Sevestrean, M. Ramalho, O. Niţescu, S. Ghinescu, S. Stoica, J. Suhonen, A. de Roubin, D. Nesterenko, A. Kankainen, P. Ascher, S. A. S. Andres, O. Beliuskina, P. Delahaye, M. Flayol, M. Gerbaux, S. Grévy, M. Hukkanen, A. Jaries, A. Jokinen, A. Husson, D. Kahl, J. Kostensalo, J. Kotila, I. Moore, S. Nikas, J. Ruotsalainen, M. Stryjczyk, and V. Virtanen, "High-precision direct decay energy measurements of the electron-capture decay of $^{97}\mathrm{Tc}$," *Phys. Rev. C*, vol. 112, p. 035501, Sep 2025. [Online]. Available: https://link.aps.org/doi/10.1103/g393-xx1w